that the relation between $\bar{P}_u$ and K is essentially independent of T_p It appears that K_n* shifts to lower values because of the temperature displacement of the stable pressure Thus, although firings at high temperatures were stable, the motor became inherently unstable at a sufficiently low value of T_p

References

[1] Jackson, F and Brownlee, W G., "The 9KS11000 rocket engine for the Black Brant III (U), Interim report—First ten firings, Part II—Ballistic design and combustion instability investigations," Canadian Armament Research and Development Establishment Tech Memo 653/62 (1962); unclassified

[2] Morris, E P, personal communication, Test and Evaluation Section, Propulsion Wing, Canadian Armament Research and Development Establishment (1963)

[3] Dickinson, L A and Jackson F, "Studies on combustion of polyurethane propellant in rocket motors," 9th Tripartite AXP Res Conf, Vol IV (April 1959); confidential

[4] Dickinson, L A, "Command initiation of finite wave axial combustion instability in solid propellant rocket motors," ARS J **32**, 643–644 (1962)

[5] Dickinson, L A, Brownlee, W G, and Jackson, F, "CARDE investigations of finite wave axial combustion instability," Canadian Armament Research and Development Establishment TN 1459/62 (1962); unclassified

[6] Brownlee, W G, "An experimental investigation of finite wave axial combustion instability (U)," Canadian Armament Research and Development Establishment Tech Memo 660/63 (1963); unclassified

[7] Morris, E P, "A pulse technique for evaluation of combustion instability in solid propellant rocket engines,' unclassified paper in course of publication by Canadian Armament Research and Development Establishment

[8] Jackson, F, personal communication, Rocket Engine Development Section, Propulsion Wing, Canadian Armament Research and Development Establishment (1963)

[9] Brownlee, W G and Marble, F E, 'An experimental investigation of unstable combustion in solid propellant rocket motors," *ARS Progress in Astronautics and Rocketry: Solid Propellant Rocket Research*, edited by M Summerfield (Academic Press Inc, New York, 1960), Vol 1, pp 455–494

[10] Price, E W, "Combustion instability in solid propellant rocket motors," Naval Ordnance Test Station NAVORD Rept 7023 (NOTS TP 2389) (1959); unclassified

FEBRUARY 1964 AIAA JOURNAL VOL 2, NO 2

Comparison of Commercial, Spherical Powder, and Wire Bundle Tungsten Ionizers

GUNTIS KUSKEVICS* AND BARRY L THOMPSON†
Electro Optical Systems, Inc Pasadena, Calif

Cesium ionization on different porous tungsten structures was measured in terms of neutral fraction, critical temperature, and flow rate in the 10^{-6}-torr range These structures included $\frac{3}{16}$-in commercial sintered ionizers with about 2-μ average pore diameter, spherical powder ionizers of 6-μ effective pore diameter, and 12- and 6-μ-diam wire bundle ionizers Conductance was measured at room temperature with nitrogen and at operating temperature with cesium vapor Ion current and neutral fraction were plotted as log$j$ or logα vs $1/T$, which allows easier extrapolation of the critical temperatures The directly heated ionizers could be operated up to 1500°C In general, the performance of ionizers improved with time of operation During this conditioning time, the critical temperature and neutral fraction decreased The best critical temperatures for all tungsten ionizers in the 10^{-6}-torr residual gas pressure at current densities between 1 and 30 ma/cm^2 were within 100°K of Langmuir's data for solid tungsten The critical temperature had a considerable spread Neutral fractions for commercial sintered, spherical powder, and fine wire bundle ionizers ranged from 0 1 to 15% but were considerably higher for coarse wire bundle ionizers The angular distribution measurements of neutral fraction were used to select the best angular position of a neutral efflux detector for neutral fraction measurements and to test the validity of the assumption that the relative angular distribution remains independent of whether a beam is being extracted

1 Review of Surface Ionization on Porous Tungsten

THE first practical cesium ionizers in the early ion sources, surface ionization detectors, and even ion propulsion devices used solid tungsten filaments or ribbons Surface ionization of the alkali metals on solid refractory metal surfaces has been reviewed recently by Zandberg and Ionov [1] A brief review of surface ionization on other solid materials was given previously [2]

Studies of porous ionizers started with the application of commercial porous tungsten in ion engines in late 1958 At the same time, theoretical studies of surface ionization on idealized porous structures determined that the desirable pore size should be less than 1 μ [3-5]

More basic experiments with porous ionizers were performed later The first of these, by Stavisskii and Lebedev,[6] used a relatively large (10-mm diam, 2-mm thick) porous tungsten disk of 70% of theoretical density, made of a very fine 1-μ grain size

The ion current-ionizer temperature curves were similar to those for solid tungsten Following the definitions of dif

Presented as Preprint 63016 at the AIAA Electric Propulsion Conference, Colorado Springs, Colo, March 11–13 1963; revision received October 7, 1963 This work has been supported by NASA Contracts NAS8 2547 and NAS8-1537 and Air Force Contract AF 33(616)-6958 Spherical powder and wire bundle ionizers were developed by H Todd and M LaChance

* Senior Scientist Associate Fellow Member AIAA
† Physicist

ferent regions of surface ionization, the ion current in the low coverage region was constant, suggesting near 100% ionization The critical temperature T_{CI} was 80° above Langmuir's data for solid tungsten at 10 ma/cm² and 50° higher at 0 25 ma/cm² The pressure was not specified, but an apparatus diagram suggests an untrapped oil diffusion pump system with operation in the 10^{-6}-torr range

The Faraday cup collector was also the accelerator electrode with its aperture about 7 mm from the ionizer Thus, sputtering of cesium and the unidentified collector material could reach the ionizer, since there was no baffling to minimize it

More extensive studies of porous tungsten ionizers at pressures below 10^{-7} torr were reported by Husmann Operation in a bakable, mercury- and ion-pumped glass system in the 10^{-8}-torr region after a short flash of the ionizer at 1700°C produced a "clean" surface

The critical temperatures for fine porous disks (2-μ pore diam) at 10 ma/cm² were only 40° to 80°C above Langmuir's data for solid tungsten For coarse disks or fine oxidized disks, the critical temperatures were about 150°C higher than I angmuir's The neutral fractions for clean, fine disks ranged from 0 5–2% at 1 ma/cm² to 7–9% at 10 ma/cm² For oxidized disks, the neutral fractions were $\frac{1}{3}$ lower Oxidation was provided by admitting oxygen to raise the total pressure to 10^{-6}–10^{-5} torr

Emissivity of sintered tungsten was measured as a function of pore size The emissivity increased with temperature from 100° to 1200°C with a slope similar to that of solid tungsten The emissivity of disks made of 0 9- to 18-μ powder at 1200°C ranged from 0 25 to 0 55 independently of powder size Mass spectroscopic analysis of the residual gas at 10^{-7} torr indicated the presence of H_2, N_2, and H_2O but no O_2 or CO_2 The sensitivity was sufficient to give an indication at 2×10^{-9} torr

The first attempt to study surface ionization as a function of ionizer grain size (or structure) gave ionization efficiencies of 94 and 97% for ionizers made of 5- and 8-μ powder, respectively Since no ion current density, critical temperature, or emissivity were given, this work could not be compared with that of other investigators [8] The atom and ion emission from a much larger 1-in -diam porous tungsten ionizer was studied by Shelton[9] using a tantalum ribbon neutral sensor At 10^{-6} torr and ion current densities of about 0 5 ma/cm², the neutral fraction ranged from 0.2 to 3% The tungsten was often oxygenated, and some cases of poisoning were observed Some data by these investigators are included in the graphs of the final section

2 Ionizer Performance Criteria

The important ionizer performance criteria[10] are ionization efficiency, ion generation energy efficiency, and lifetime Since the ionization efficiency is usually very close to 100%, more accuracy is obtained by measuring the neutral fraction, defined as the ratio of neutral cesium efflux to total cesium efflux The ion generation energy efficiency is a measure of thermal losses due to radiation from the ionizing surface, radiation and conduction losses from the supporting structure, and leads For evaluation of the ionizer material, only the thermal radiation from the ionizing surface is of importance However, in a small single-button device other losses predominate The radiation loss from the active area is best obtained by measurement of the minimum operating temperature and the total emissivity The minimum operating temperature is equal to the so-called critical temperature For porous tungsten ionizers in 10^{-6}-torr vacuum, most good ionizers have a rather sharp critical temperature and a very small difference between the lower and upper critical temperature (hysteresis) determined from the ion current-ionizer temperature curve For many ionizers, ion current starts a sharp decline at the same time as the neutral fraction starts to rise Some ionizers, however, showed a minimum in neutral fraction at a temperature higher than the critical temperature for the ion current The ion current critical temperature T_{CI} is most conveniently defined as that temperature at which the current has decreased by 5% from its maximum value This is discussed in more detail below

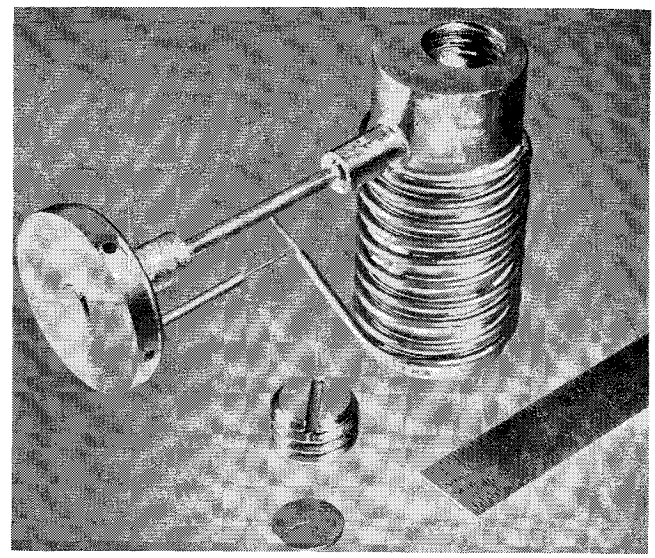

Fig 1 Ionizer reservoir assembly

The total emissivity can be measured in a separate experiment using the same material It is assumed here that the differences due to emissivity are smaller than the effect of the spread in the critical temperatures and that they would favor high-emissivity ionizers

Some indication concerning the life of the ionizers can be obtained by observing time trends in their gas and cesium permeability, neutral fractions, and critical temperatures Only limited data were obtained because of the short duration of most tests Many of these tungsten ionizers were operated for over 100 hr between 1400° and 1500°C without any decrease of permeability

3 Ionizer Test Apparatus

Nearly all ionizers tested were disks of $\frac{3}{16}$-in diam × 0 040-in thick They were brazed into a molybdenum holder, as shown in Fig 1, using an Mo-C-B braze This ionizer assembly was mounted into a single-aperture ion accelerator using a 45° beam-forming electrode and planar accel-decel electrodes, as shown in Figs 2 and 3

A few grams of cesium were loaded into the reservoir using regular dry box techniques Upon removal of the ionizer assembly from the dry box, the cesium in the reservoir was under 1 atm pressure of nitrogen The low permeability of the porous ionizer was the only barrier against the infusion of air while the assembly was mounted into the accelerator and transferred into the vacuum test chamber

The ionizer-accelerator assembly was placed in a 1 × 3-ft vacuum tank that was equipped with either a stationary or a movable neutral detector, a liquid-nitrogen-cooled ion collector, and a liquid-nitrogen-cooled liner Operating pressure was in the 10^{-6}-torr range A schematic view of the neutral eye is also shown in Fig 2 and the ion collector in Fig 4 The ionizer temperature was measured by a W5%Re-W26%Re thermocouple in a $\frac{1}{16}$-in -o d tantalum sheath The hot junction was in a deep hole in the ionizer holder and very near to the ionizer disk The other end of the thermocouple passed through the vacuum wall without interruption by means of a gasketed feedthrough

The cesium reservoir temperature was monitored by a bare iron-constantan thermocouple near the exit of the massive nickel reservoir

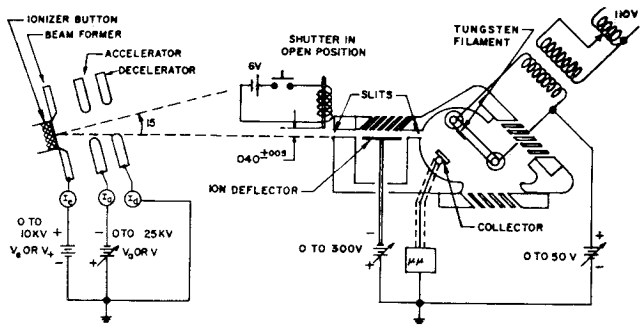

Fig 2 Schematic and circuit diagram of ion accelerator and neutral detector

4 Ionizer Test Procedure

The gas conductance of most ionizers was measured before and after brazing into the holder and again after the ionizer tests The ionizer and reservoir heaters were turned on at the same time as all instrumentation and high voltages The neutral eye filament was baked out at 1600°C until the background reading with the shutter closed was a few nanoamps The operating temperature was between 1100° and 1300°C, depending upon atom incidence rates The ionizer was heated at about 1300°C

The ion collector current was monitored to establish the proper cesium-reservoir temperature for a reasonable ionizer-current density, say, 5 ma/cm² With the reservoir temperature and cesium flow stabilized, the accelerator/ionizer voltage ratio for proper focusing was checked visually by observing the ion beam impact area at the collector or by observing the beam at 10^{-5} torr of argon Usually the accelerator voltage was twice the value of the ionizer voltage, and the beam was 1–2 in in diameter at the collector

With proper focusing, the current-voltage characteristic was taken to insure emission-limited operation This was done for each new current density and is very important at the high current densities when operation is very near to being space-charge limited The movable neutral detector was usually located at 15° to the ion beam axis and 6 in from the ionizer The movable detector had 0 020-in -wide slits The stationary detector had 0 040-in slits and was only 3 in from the ionizer If the neutral fraction was below 10%, indicating that the ionizer had been properly conditioned, the angular dependence of α was checked to see that it was fairly constant and that the probe was located at the proper angle for reliable results Operation too close to the beam or too much in the shadow of the electrodes gave erroneous results

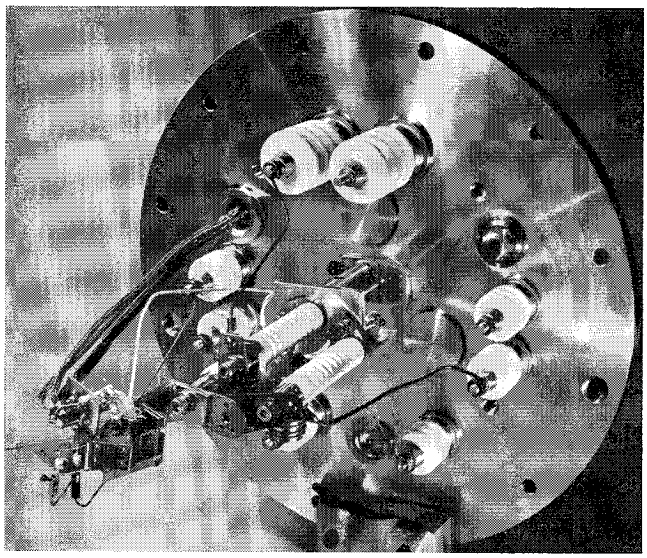

Fig 3 Ionizer testing equipment including neutral detector

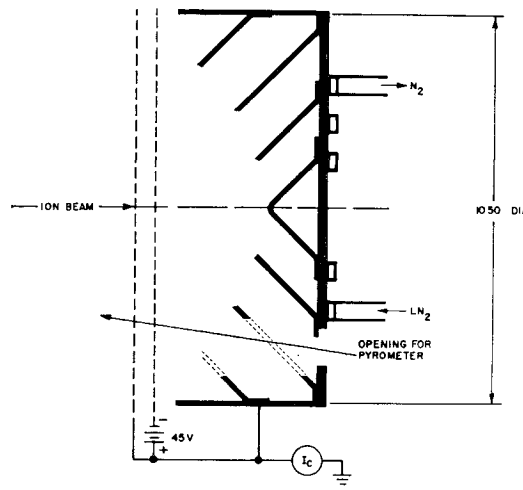

Fig 4 Conical baffle current collector with electron impression

The neutral fraction was obtained by measuring the neutral detector current with accelerating voltage on and off, subtracting background readings obtained by operating the shutter After the proper probe angle was checked, the ion current and neutral fraction were measured as a function of ionizer temperature for a series of current densities The dependence of cesium permeability upon the ionizer temperature was also obtained, since it is related to the ion current density j The j vs T curves were taken repeatedly to observe reproducibility, hysteresis, and time trends

After each test, the ionizer was inspected and its nitrogen conductance checked Three types of tungsten ionizer structures were tested: 1) commercial sintered ionizers designated by the symbol *SW*, 2) spherical powder ionizers designated *SP*, and 3) wire bundle ionizers designated *WB*

5 Ionizer Nitrogen Conductance Permeability and Braze Infiltration

Nitrogen conductance measurements using electronic timer equipment provided a fast and simple method to check and sort large numbers of unmounted porous ionizers The actual measurement determined the time for the pressure in a constant volume to drop about 1% of the pressure difference across the ionizer The inverse of this time is proportional to the conductance of the sample Conductance depends upon both the area and the thickness Both can be easily measured for unmounted ionizers and used to calculate permeability The permeability value is independent of sample area and thickness and depends only upon the material The distribution of permeability for a large number of ionizers is indicative of the ionizer material uniformity The gas permeability is a much more sensitive indicator of material quality than apparent material density Change in permeability with time at high temperature provides an indication of structural instability For ionizers brazed into a holder, the open area is no longer definite due to braze infiltration, and it is impossible to calculate gas permeability One can assume that the permeability

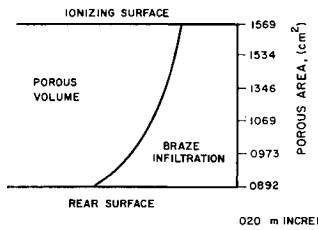

Fig 5 Braze penetration into spherical powder ionizer as measured from a cross section metallograph, *SP2*, A = 0 179 cm²

Table 1 True and apparent permeability for spherical powder ionizers

Ionizer identity	True permeability $K = \frac{\Delta m}{\Delta p}\frac{\Delta x}{A}\frac{1}{\Delta t}$, g/(cm-torr-sec), $\Delta x/A = 0\ 5705$	Apparent permeability after brazing K_1, g/(cm-torr-sec)	Apparent permeability after test K_2, g/(cm torr-sec)	$(K - K_1)/K = (A - A_1)/A$	Cesium flow j, ma/cm² at 300°C, $A_1/0\ 157$ cm²
*SP*1	1 42 × 10^{-6}	0 37 × 10^{-6}	0 437 × 10^{-6}	0 74	3 50
*SP*2	0 92	0 493	0 632	0 462	4 47
*SP*3	1 17	0 628	0 624	0 464	3 78
*SP*4	1 17	0 553	0 488	0 528	1 0
*SP*5	0 92	1 21		(−0 315)?	
Average	1 12	0 650	0 554	0 548	

of an unmounted ionizer does not change during brazing, if the brazing temperature is considerably lower than the sintering temperature

The nitrogen conductance was checked before performance testing These tests are also useful for the detection of leaks after brazing, cracks upon testing, braze penetration, or changes of permeability Care must be taken to remove all cesium, its oxides, and cleaning fluid from the ionizer after testing, since these can effectively seal the ionizer pores Most ionizers were baked out in vacuum after their performance testing

The conductance was measured before and after brazing the ionizer into a holder The permeability was calculated from the unmounted ionizer measurement An apparent permeability was calculated for the mounted ionizer, using the same area and thickness value The ratio of the true and apparent permeability then gives the ratio of initial to effective post brazing area Table 1 shows true permeability, apparent permeability before and after performance testing, and the closed area fraction and cesium permeability represented by j at 300°C for the *SP* ionizers From this table the fraction of ionizer area closed by brazing varies from 46 to 74% with an average 55% closure The ionizer holder produces a braze infiltration pattern, as shown in Fig 5 From Fig 5 and the column of porous area, one can see the extensive braze infiltration at the rear surface The gas conductance should be determined by the average cross-sectional area near the center of the ionizer The braze closure varies from 12% at the front surface to 50% at the rear surface, whereas the gas conductance closure was 46% Hence, the gas conductance is determined more by the minimum open cross section than by a geometric average

The apparent nitrogen permeability of the average *SP* ionizer is two to three times that of the average *SW* ionizers The *WB* ionizers are about 10 times more permeable

The commercial sintered tungsten ionizers (designated by the symbol *SW*) were selected from a large number of buttons to have a range of permeabilities convenient for a reasonable cesium reservoir temperature and a fine and stable pore structure The average spherical powder ionizers (designated by the symbol *SP*) and the wire bundle ionizers (designated by *WB*) were made by H Todd and M LaChance of Electro-Optical Systems, Inc , under a NASA contract

6 Cesium Permeability and Its Change with Temperature

A measure of cesium conductance can be obtained in two ways: 1) by using the cesium atom probe, and 2) by measuring cesium ion current The neutral probe current was measured for two *SW* and two *WB* ionizers used for the study of angular distribution of the cesium effusion pattern The probe current on the ionizer axis was assumed to be directly proportional to the total cesium flow in particles per second Data showed that the cesium conductance of *WB* ionizers was about 50 times that of *SW* ionizers Each group has a spread of factors up to 10

The second type of cesium conductance estimate is the ion current density in Fig 6, which does not include neutrals For *SW* and *SP* ionizers, the actual cesium conductance in equivalent milliamperes per square centimeter was 1–15% higher and for *WB* about 5–50% Note also that higher current densities required higher ionizer temperatures The cesium conductance is slightly dependent upon the ionizer temperature, as seen in Fig 7 The ionizer was not held at constant temperature in Fig 6 The ion current measurement gives the value of cesium conductance which is converted to an apparent cesium permeability measurement by normalizing to equal areas for each of the ionizer groups The best estimates of the active areas are 0 157 cm² for *SW* and *SP* ionizers, except for *SW*1, which was 0 220 cm², and 0 141 cm² for *WB* ionizers The *SP* ionizers have apparent cesium permeabilities three times higher and the *WB* about 10 to 20 times higher than the *SW* ionizers

The change of cesium conductance with temperature can be measured with the atom probe, assuming that the angular distribution does not change with ionizer temperature Figure 8 shows the decrease of ionizer permeability with temperature as measured by the neutral probe on the geometric axis In this case there is no voltage applied and no surface ionization, and there is a high surface coverage The equivalent ion current density indicated for each curve gives the average ion current that would be generated at this flow rate (or cesium temperature) with 100% ionization The temperature coefficients of conductance shown were computed at $T = 1200$°C

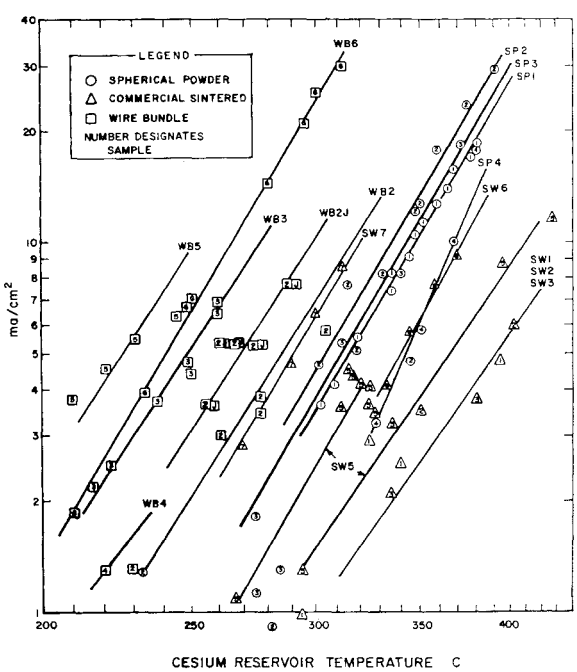

Fig 6 Cesium current density as a cesium permeability indicator for the various tungsten ionizers

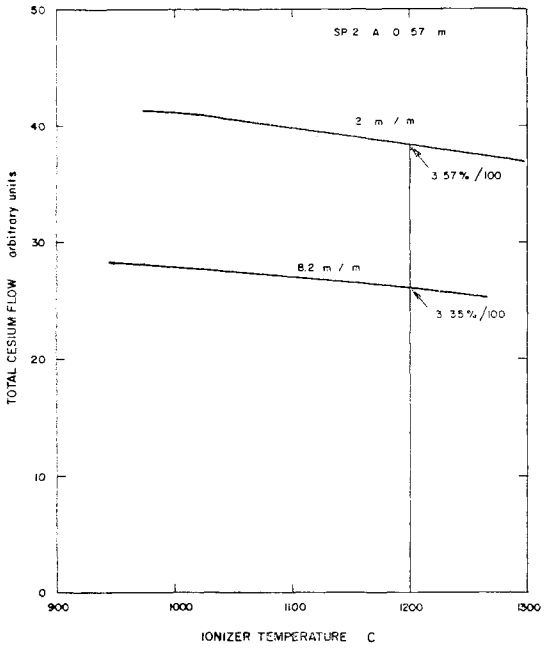

Fig 7 Change of cesium permeability with ionizer temperature at high surface coverage

7 Active Ionizer Area and Ion Current Density Measurement

Measurement of the active ion-emission area is needed for the calculation of ion current density The active area can be estimated 1) by microscopic observation of ionizer surface for a color change around the edges; 2) by comparison of nitrogen conductance before and after brazing into the holder; 3) by obtaining a sputtering pattern in a parallel plane arrangement; 4) by low magnification ion microscopy; and 5) by a photomicrograph of the ionizer cross section, which destroys the ionizer The first method is the simplest but is not very reliable The second method gives the relation between true and apparent nitrogen permeability but does not give an accurate measure of active area as discussed in the previous section

A more reliable method is the measurement of active emission area by the sputtering pattern. The ionizer is placed into a plane parallel diode arrangement with a copper cathode and a gap of about 0 175 in Emission-limited operation is maintained to assure parallel ion trajectories This produces

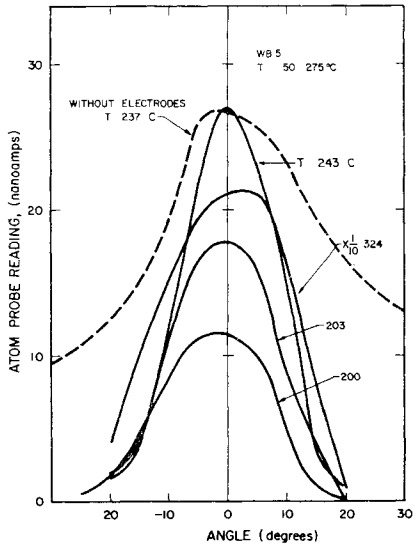

Fig 8 Angular distribution of atoms through electrodes

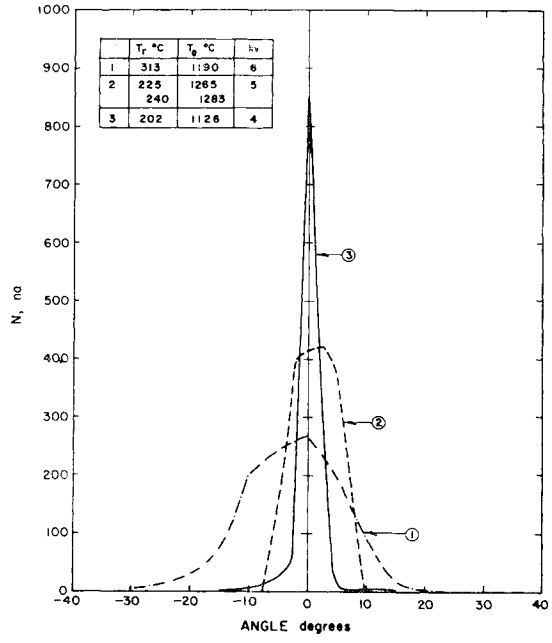

Fig 9 Ion beam profiles for a wire bundle ionizer

a well defined sputtered area that is assumed to be equal to the active ion-emission area The sputtering pattern area for *SW*7 was 0 155 cm², compared to 0 157 cm² measured by metallographic cross section for *SP*2 Based on these two measurements, active areas for early *SW* and *SP* ionizers were assumed to be 0 157 cm² and measured for all recent ionizers

For the wire bundle the surface closure measured on a metallographic cross section was 15 2%, and the penetration pattern was different The 0 141-cm² area was used for most 12-μ wire bundles For the fine wire bundle, the sputtering pattern gave an area of 0 114 cm² or a 23% closure

The measurement of ion current is made at a collector and involves the following assumptions:

1) The entire beam emerging from the engine is collected This is checked by a visual observation of the target luminescence area, usually from 1 to 3 in in diameter The collector diameter is 10 in It can also be checked by visual observation of the beam angle in argon A third check is provided by the *I-V* characteristic When some of the beam misses the target, this fraction usually depends upon the voltage and produces an irregular *I-V* curve

2) There is no secondary electron-emission current away from the collector This is checked by increasing the secondary electron-suppressor voltage until the collector current no longer decreases

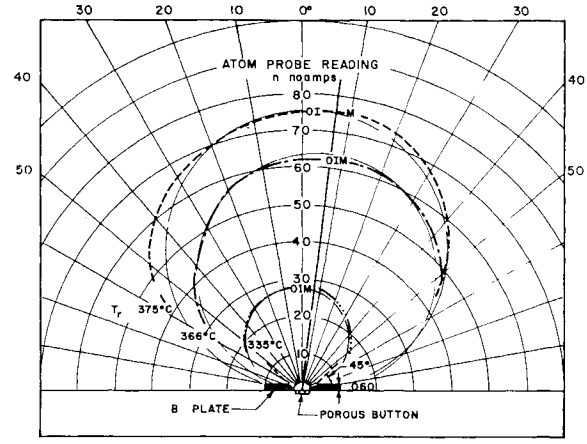

Fig 10 Angular distribution of cesium atoms evaporating from a commercial sintered porous tungsten ionizer as a function of cesium flow rate, *SW*3, *T* = 1200 C

3) There is negligible interception of the emitted ions by the accelerating structure Ion interception at the accel electrode is small but measurable Measurements are complicated by electron currents

The active surface area measurement includes the following additional assumptions:

1) Emission is from the apparent geometrical area, without regard to the ratio of pore area to closed area or to any true solid area dependent on roughness and grain structure of the surface

2) There is no emission from the brazed area or the holder Most of the preceding factors would tend to increase the current density; hence our measurements reflect a conservative value

A typical current-voltage characteristic is shown in Fig 9 The ratio of accelerator V_- to ionizer V_+ voltage is kept constant and equal to 2 This is equal to an accel-decel ratio $(V_- + V_+)/V_+$ of 3 The accelerator perveance for this curve is 1 0 nperv of 6 5 nperv/cm^2, using for the area the active area of 0 157 cm^2 corresponding to a braze infiltration of 12%

8 Angular Distribution of Atoms, Neutrals, Ions, and Neutral Fraction

An important ionizer performance figure of merit is the neutral fraction The neutral fraction is defined as the ratio of neutrals to the total efflux of cesium ions and neutrals The term "neutrals" in this report will be used specifically for the case where the accelerating voltage is applied and an ion beam is being extracted The term "atoms" will be used for the case where no accelerating voltage is applied and the entire efflux is atoms

Since, with the use of a probe, a small portion of the neutral fraction rather than the total is measured, one must ascertain whether the neutral fraction is independent of the angle For this reason the angular distributions of neutrals, atoms, and neutral fractions were studied in detail In some of the measurements the slit widths were 0 040 in with a notched tungsten filament In some of the latter experiments the slit widths were reduced to 0 020 in and the notches eliminated in order to reduce the chance of systematic angular error

The angular distribution of cesium atoms evaporating from a commercial sintered porous tungsten ionizer without any accelerating structure is shown in Fig 10 as a function of the flow rate This distribution is very nearly cosine It is typical for most measurements of this type, and it was independent of the cesium flow rate and of the ionizer temperature The angular distribution of cesium atoms evaporating from a wire bundle showed a very definite peak, and it deviated more from the cosine law depending upon the nature of the mechanical surface treatment Figure 11, for example, shows a highly peaked pattern obtained with an etched wire bundle The etching has opened up the pores Distributions for some of the other wire bundle ionizers were not as highly peaked because their surface pore openings were reduced by mechanical abrading or by compression of the button This definitely suggests that the atoms evaporating from a wire bundle come to some degree from within the pores A shielding effect of the electrode on the distribution of atoms is shown in Fig 8 or from comparison with the curve for the case without electrodes A complete study of the angular distributions of ions, atoms, neutrals, and neutral fraction through electrodes for a wire bundle *WB5* is shown in Fig 12 These curves illustrate that the neutral fraction cannot be measured with this probe inside of the ion beam, which is about 18° wide The signal due to ions is considerably larger than that due to atoms or neutrals The neutral detector can be used for a study of ion beam profiles illustrated in Fig 9 on a rectangular plot These curves illustrate the ion beam expansion from a total included angle of 8° to about 30° as the current density is increased from about 3 to about 12 ma/cm^2, even though the voltage is also increased

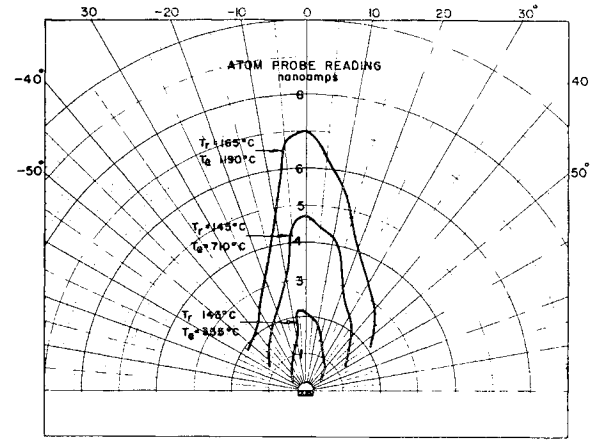

Fig 11 Angular distribution of cesium atoms as a function of ionizer temperature, etched *WB5*

Either a single screen accelerating electrode or a set of slotted accel-decel electrodes was used to measure the angular dependence of the neutral fraction In both cases, the neutral fraction appeared reasonably constant within an angle of about 20° just outside of the ion beam and before the signal strength fell off to a very low value Most of the checks of the constancy of neutral fraction with angle were done in the presence of the regular electrodes A set of curves for a wire bundle including neutral fraction was already shown in Fig 12 A set of neutral fraction curves for a large range of current densities is shown in Fig 13 As seen from these curves, there is always a range of angles, just outside of the beam before the signal strength declines into the noise level, in which the apparent neutral fraction is relatively constant Observe also that the range changes with the current density At higher current densities the beam expands more, and the neutral eye must be located at a large angle or made insensitive to the presence of the energetic ions The 15° position of the neutral detector appears to be adequate for current densities of up to about 15 ma/cm^2

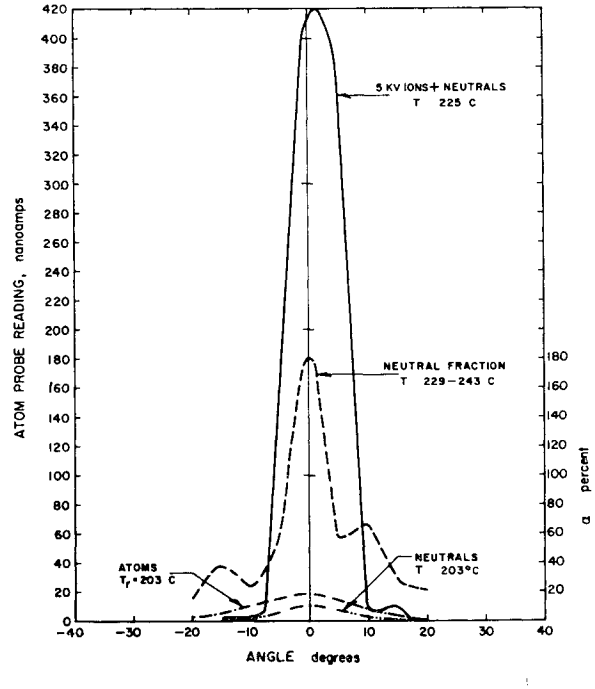

Fig 12 Angular distribution of ions, atoms, neutrals, and neutral fraction through electrodes, *WB5*

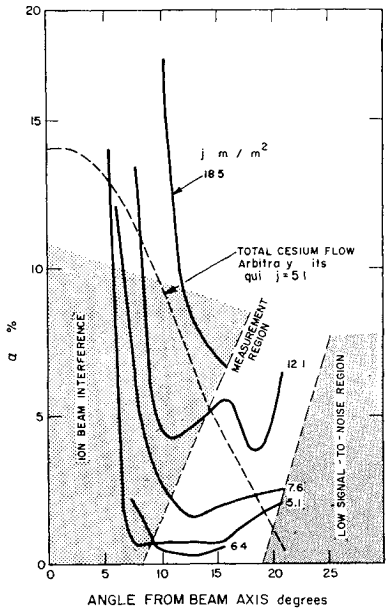

Fig 13 Angular dependence of apparent neutral fraction and total cesium flow (as neutrals) for spherical powder ionizer, *SP*2

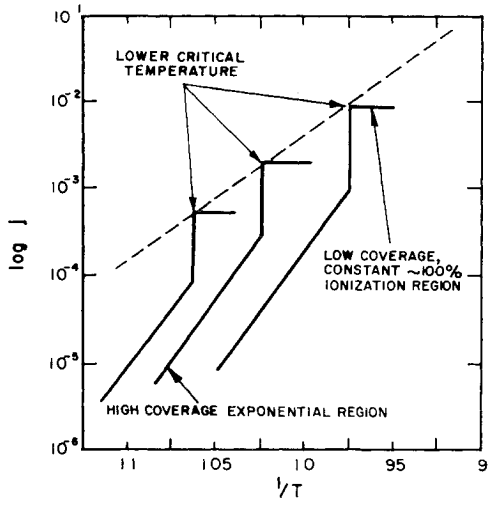

Fig 14 Definitions of surface ionization regions for ion current-ionizer temperature curves for solid tungsten

9 Ion Current Density, Neutral Fraction, and Critical Temperatures

The most popular measurement in surface ionization is the ion current density as a function of ionizer temperature for various cesium flow rates A set of typical curves for solid tungsten as measured by Langmuir[11] is shown in Fig 14 to define the various regions of operation These data are usually taken with decreasing temperatures At high temperature the cesium coverage is low, and for high work function surfaces the ionization is so nearly 100% that it appears essentially constant At a certain temperature, called the critical temperature, the ion current discontinuously drops by more than a decade as the surface becomes covered with cesium In the high-coverage region the decline is exponential

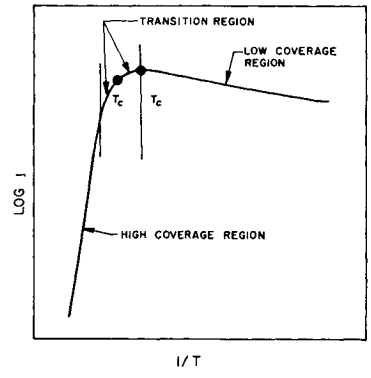

Fig 15 Definitions of surface ionization regions for cesium on typical porous tungsten ionizers

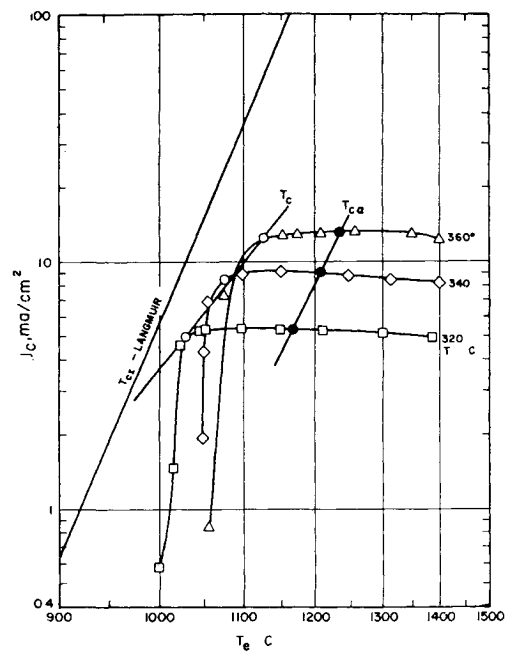

Fig 16a Log j vs $1/T$ curves defining two "critical temperature" points for *SP*1 ionizer

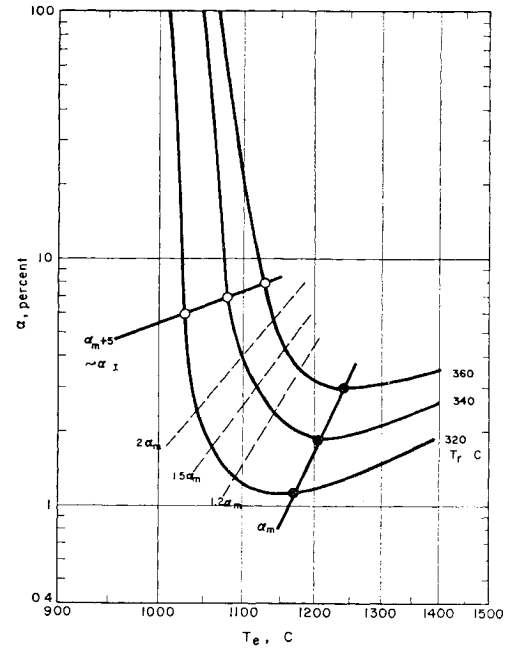

Fig 16b Log α vs $1/T$ curves showing neutral fraction corresponding to curves in Fig 16a

For the porous ionizer, the typical current-temperature curve is more like that in Fig 15 The low-coverage region is most likely no longer constant because of a change in ionization efficiency and ionizer permeability with ionizer temperature Instead of a discontinuity, there is a transition region characterized by a large change in the slope There are sometimes two "critical temperatures": one, T_{CI}, defined as the temperature at which the ion current has declined by 5%, and the other, T_C, defined as the temperature corresponding to minimum neutral fraction

A typical set of selected data for *SP*1 ionizer illustrates the various definitions and graphing techniques in Fig 16 The

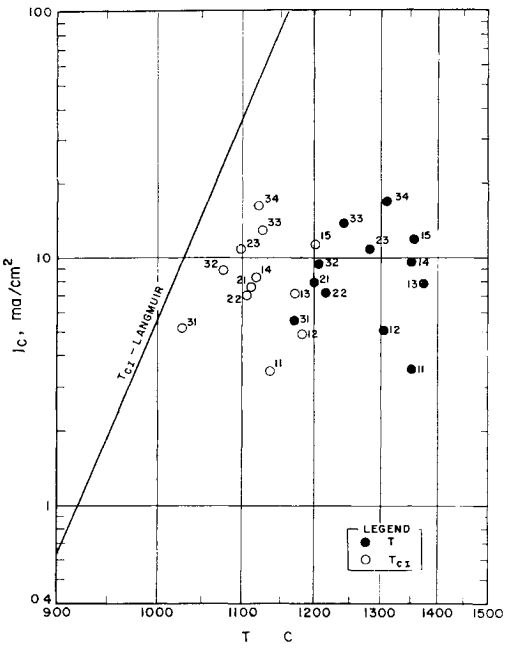

Fig 17a Log j vs $1/T_c$: summary of all critical points for $SP1$ ionizer

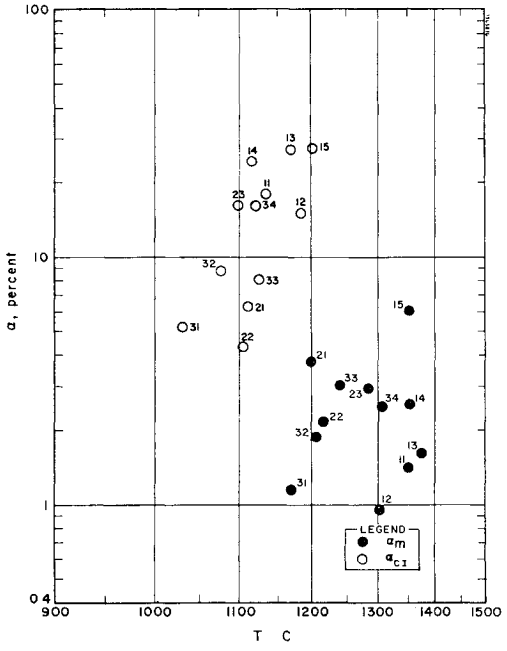

Fig 17b Log α vs $1/T$: summary of all critical points for $SP1$ ionizer

current density j is based upon an area of 0 179 cm² and was not corrected for 12% braze closure Hence, the true ion current density is 12% higher All curves were taken with decreasing ionizer temperatures, and the T_{CI} points are the lower critical temperature, which may be below the minimum operating temperature for the ionizer The transitition with increasing temperatures can occur at a higher temperature (about 10–30°) called the upper critical temperature The $\log j$ vs $1/T$ plots are used because, for solid tungsten, the T_{CI} points fall on a line marked T_{CI}-Langmuir The T parameter indicated is the temperature of the cesium reservoir in degrees Centigrade

Simultaneous with the ion current, the neutral fraction is measured, and the corresponding points are plotted in Figs 16a and 16b Sometimes the temperature $T_{C\alpha}$ corresponding

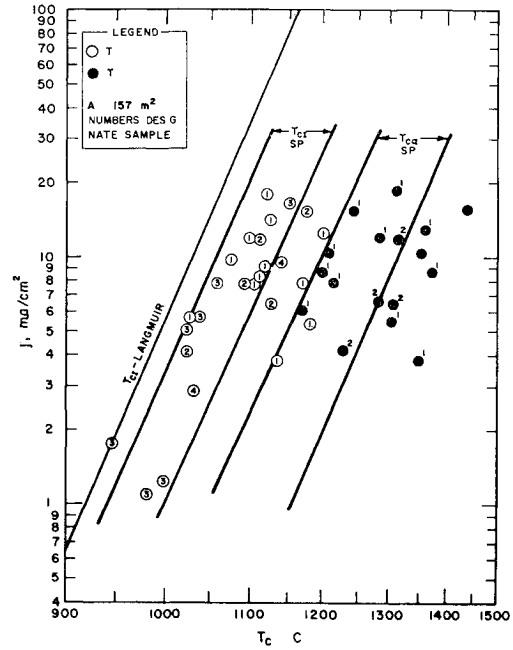

Fig 18 Summary of current and neutral fraction critical temperature points for four spherical powder ionizers

to a minimum neutral fraction of the $SP1$ ionizer should be operated at least 100°C hotter than the T_{CI} line The T_{CI} points in the j vs $1/T$ plot coincide closely to the $\alpha_m = +5\%$ line in the α vs $1/T$ plot If 6–8% neutral fractions cannot be tolerated, the ionizer must be operated at a temperature above the T_{CI} line However, one does not have to go to α_m As the lines $1\,2\alpha_m$, $1\,5\alpha_m$, and $2\alpha_m$ indicate, the change of α near the minimum is very slow A 30° increase in temperature decreases α by more than 50% Optimum ionizer operation is, therefore, close to the T_{CI} line and between T_{CI} and $T_{C\alpha}$ in Fig 16a, corresponding to about the $1\,5\alpha_m$ line in Fig 16b

Figures 17a and 17b contain a summary of all critical temperature points for $SP1$ ionizer obtained from points on all curves similar to those in Figs 16a and 16b The number with each point indicates the day and order in which the curves were taken For example, 32 was taken during the third day of testing, and it is the second curve Such graphical summaries of critical points for each ionizer with the order identified show the time trends, especially during the initial period of ionizer conditioning As seen by comparison with Fig 16a, the critical temperature T_{CI} and $T_{C\alpha}$ has decreased by about 100° from the first day to the third day Figure 17b summarizes all neutral fraction values α_{CI} corresponding to $T_{C\alpha}$, showing the time measurements The α_m values for this ionizer are much lower than the α_{CI} The α_{CI} is very nearly equal to $\alpha_m + 5$ For this ionizer, curves on the first day showed no definite minimum up to 1300°C, and their slopes were lower

To establish the performance of a given porous structure, several ionizers of the same structure must be tested The current and neutral fraction vs critical temperature points of four spherical powder ionizers are shown in Fig 18 Neglecting the points measured during the conditioning period, the current vs critical temperature points are in a band marked T_{CI}-SP This band is about 75°C wide and starts about 25°C above the Langmuir line The neutral fraction critical temperature points fall in a similar band marked $T_{C\alpha}$-SP which is 125°C wide and starts about 150°C above the Langmuir line

A similar summary of T_{CI} points for commercial sintered tungsten ionizers, given in Fig 19, shows a larger spread For most SW ionizers, the $T_{C\alpha}$ points were identical with T_{CI}

A typical set of ion current density and neutral fraction curves for a 12-μ wire bundle ionizer with critical temperature

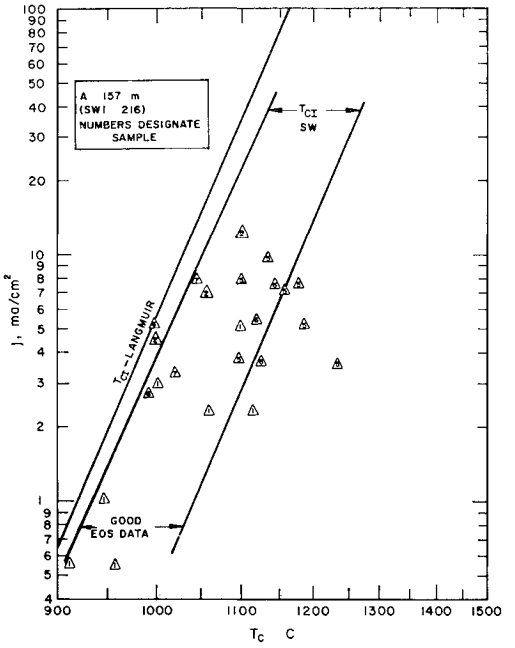

Fig 19 Summary of T_{CI} points for five commercial sintered tungsten ionizers

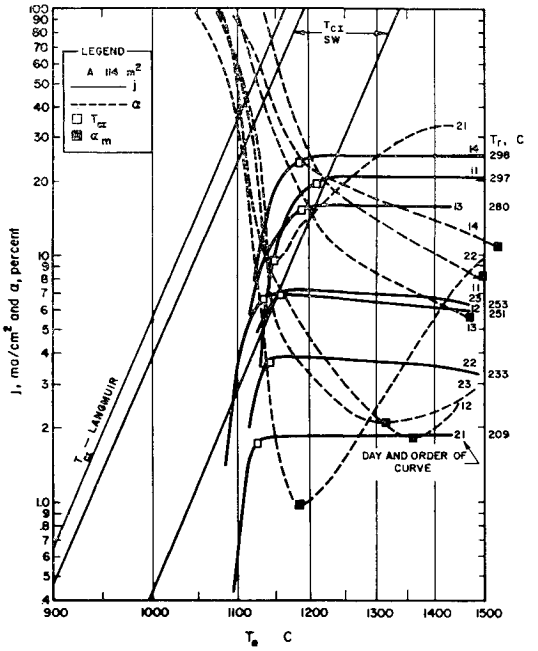

Fig 21 Ion current and neutral fraction vs ionizer temperature for fine wire bundle *WB6*

points is shown in Fig 20 Note the much higher neutral fractions and the coincidence of most T_{CI} and $T_{C\alpha}$ points except at low α values

The fine wire bundle ionizer α curves in Fig 21 showed much more pronounced minima, especially at low flow rates Because of ionizer-to-reservoir heat flow, the reservoir temperature depended upon the ionizer temperature The nature of the α curves changed with ionizer conditioning Numbers with each curve again indicate their order

The logα vs T_e graphs (Fig 16b) are most useful in establishing the neutral fraction critical temperature $T_{C\alpha}$ and the values of α_{CI} at the ionizer critical temperature To compare the neutral fractions of various ionizers and structures, a plot of α vs j is used Figure 22 shows the minimum neutral fraction of several ionizers for the various porous tungsten structures Some of the spread for each ionizer is caused by the time dependence illustrated in Fig 23 Note the large reduction during the initial conditioning and the smaller change on each successive day The commercial porous tungsten ionizers, except for *SW5*, and the spherical powder ionizers generally have neutral fractions ranging from a fraction of a percent to 10% at 30 ma/cm² This is higher than given by the Langmuir data for solid tungsten The large neutral fractions of the 12-μ wire bundle ionizers are probably due to the opening of the pores at high temperatures and the appearance of small surface cracks The fine wire bundles made of 6-μ-diam wire had much lower neutral fractions than the coarse wire bundles, after an initial conditioning period of about 1–2 hr

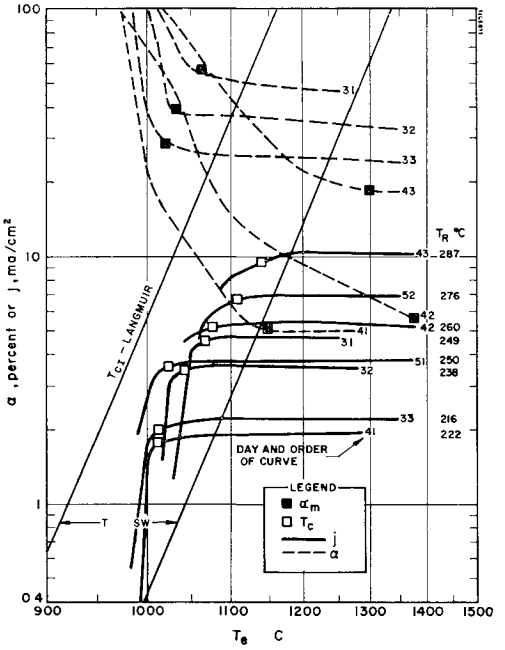

Fig 20 Ion current and neutral fraction vs ionizer temperature for coarse wire bundle *WB3*

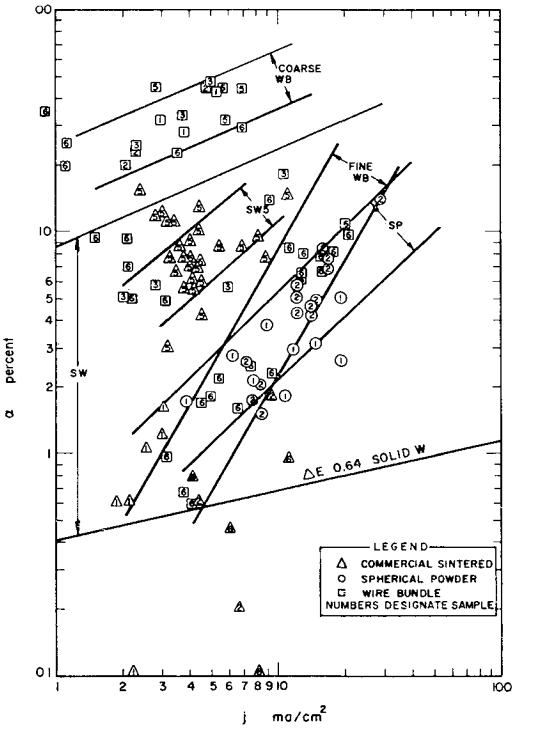

Fig 22 Neutral fractions for various porous tungsten structures

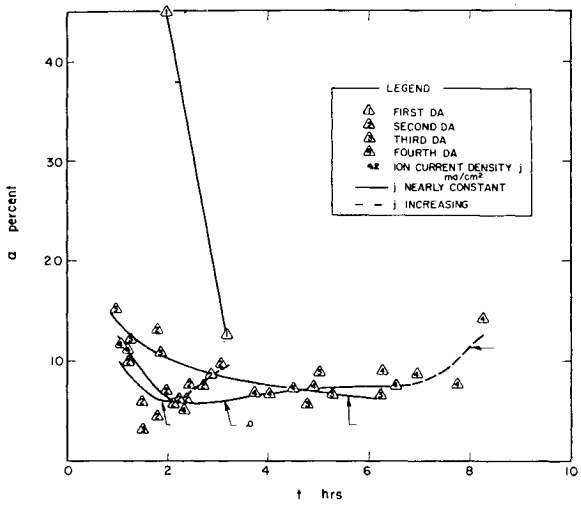

Fig 23 Time dependence of neutral fraction *SW*5

10 Comparison of Commercial, Spherical Powder, and Wire Bundle Ionizers

In Fig 24, surface photomicrographs show the pore sizes and distances for typical ionizers of each type The commercial porous tungsten has irregular pore sizes and shapes with an equivalent diameter of 2 4 μ, and an average pore distance of 6 7 μ The spherical powder ionizers have more regular slitlike pores with areas for which the equivalent diameter is 6 4 μ The average pore distance, assuming a regular distribution into a hexagonal close-packed array, is 13 5 μ The coarse wire bundle has some very large pores of about 15μ with an average of about 4 μ For most coarse *WB* ionizers made of 0 0005-in -diam wire, the wire ends were expanded mechanically at the surface to reduce the pore size and produce uniform packing Operation at high temperature tended to open up the pores The fine wire bundle made of 0 00025-in -diam wire had a 0 3-μ equivalent pore diameter

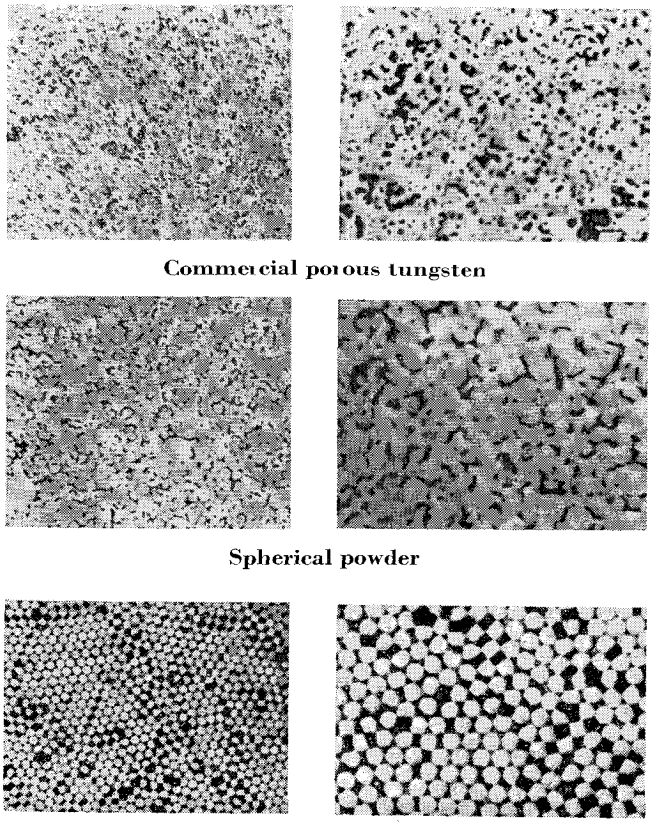

Commercial porous tungsten

Spherical powder

Wire bundle

Fig 24 Set of comparative surface photomicrographs

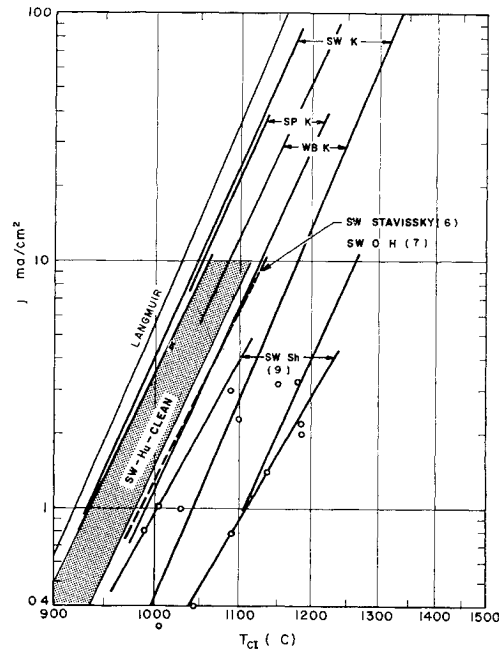

Fig 25 Comparison of critical temperatures for 1) commercial ionizers, 2) spherical powder, and 3) wire bundle ionizers

The apparent nitrogen permeability of all ionizers is compared in Table 2 The average *SP* ionizer was about 4 times the average *WB* ionizer, and about 10 times more permeable to nitrogen than the average *SW* ionizer The cesium conductance at operating temperature as given by ion current density in Fig 6 follows a similar pattern, but the spread is larger for the atom detector data and smaller for the ion current density data The change of permeability with the ionizer temperature was about 3%/100°K for all structures

The angular distributions of atoms indicated evaporation from the surface for *SW* ionizers and from the surface for *WB* ionizers with small pore sizes or from within the pores for *WB* ionizers with large pore sizes

Table 2 Apparent nitrogen permeability of mounted ionizers

Ionizer identity	K, 10^{-6}g /(cm torr-sec)
Commercial sintered	
*SW*1	0 078
*SW*2	0 122
*SW*3	0 226
*SW*4	0 186
*SW*5	0 257
*SW*6	0 285
*SW*7	0 570
Average	0 246
Spherical powder	
*SP*1	0 37
*SP*2	0 493
*SP*3	0 628
*SP*4	0 553
*SP*5	1 21
Average	0 650
Wire bundle, 12μ	
*WB*1	1 41
*WB*2	1 37
*WB*3	2 90
*WB*4	3 34
*WB*5	
Average	2 25
Wire bundle, 6μ	
*WB*6	2 58

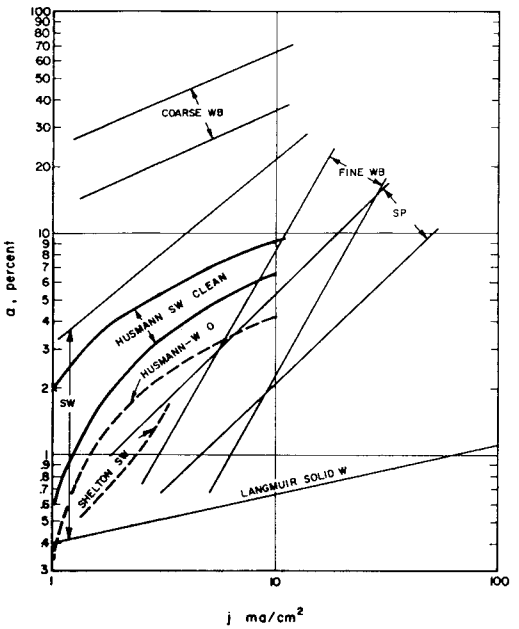

Fig 26 Comparison of neutral fractions of the various tungsten structures with results of other investigations

The critical temperatures of all *SP* ionizers given in Fig 18 demonstrate the spread of points from sample to sample and the difference between T_{CI} and $T_{C\alpha}$ Such differences were not observed for the *SW* ionizers in Fig 19 or for most of the 12-μ wire bundles as in Fig 20 A very pronounced minimum was observed in α at $T_{C\alpha}$, which was very nearly equal to T_{CI} for the 6-μ wire bundle in Fig 21

A comparison of current vs critical temperature T_{CI} data for all tungsten structures with data published by other investigators is given in Fig 25 Nearly all tungsten ionizers fall within a band that is between about 30° and 130°C above the Langmuir line The data taken during initial conditioning periods are neglected The spread for *SP* and *WB* ionizers is smaller (about 90°C) as compared to the *SW* ionizers

Similar distributions of points are found in the α vs j data of Fig 21 These same data are summarized and compared with results of other investigators in Fig 26 The coarse wire bundle ionizers had very high neutral fractions, and the commercial porous tungsten showed a very large spread The spherical powder ionizers had a narrow spread with values similar to the fine wire bundle The highest ion current density was reached with the *SP* ionizers, the fine wire bundle being next highest Again all data, except the band due to Hussman and marked *SW*-clean, were obtained at 10^{-6}-torr residual gas pressure where the surfaces are probably oxygenated

Performance tests are continuing, and some ionizers of each type will be tested at lower residual gas pressures in an ultrahigh vacuum system The more regular structures, such as the fine wire bundle and the spherical powder ionizers, have given better performance than the commercial sintered tungsten, but a final comparison should include data on more samples and at lower residual gas pressures

References

[1] Zandberg, E Ya and Ionov, N I, "Surface ionization," Usp Fiz Nauk **67,** 581–623 (1959)

[2] Kuskevics, G, Worlock, R M, and Zuccaro, D, "Ionization, emission and collision processes in the cesium ion engine," *ARS Progress in Astronautics and Rocketry: Electric Propulsion Development,* edited by E Stuhlinger (Academic Press Inc, New York, 1963), Vol 9, pp 229–267

[3] Zuccaro, D, Speiser, R C, and Teem, J M, 'Characteristics of porous surface ionizers," *ARS Progress in Astronautics and Rocketry: Electrostatic Propulsion,* edited by D B Langmuir, E Stuhlinger, and J M Sellen Jr (Academic Press Inc, New York, 1961), Vol 5, pp 107–139

[4] Nazarian, G M and Shelton, H, "Theory of ion emission from porous media," *ARS Progress in Astronautics and Rocketry: Electrostatic Propulsion,* edited by D B Langmuir, E Stuhlinger, and J M Sellen Jr (Academic Press Inc, New York, 1961), Vol 5, pp 91–106

[5] Reynolds, T W and Kreps, L W, 'Gas flow, emittance and ion current capabilities of porous tungsten," NASA TN D-871, 43 pp (August 1961)

[6] Stavisskii, Yu Ya and Lebedev, S Ya, "Surface ionization of cesium upon diffusion through porous tungsten," Zh Tekh Fiz **30,** 1222–1226 (1960); also Soviet Phys—Tech Phys **5,** 1158–1161 (1961)

[7] Husmann, O K, 'Experimental evaluation of porous materials for surface ionization of cesium and potassium," *ARS Progress in Astronautics and Rocketry: Electric Propulsion Development,* edited by E Stuhlinger (Academic Press Inc, New York, 1963), Vol 9, pp 195–217

[8] Hubach, R A and Seele, G D, "Properties of porous tungsten and ionization of cesium," IAS-ARS Preprint 61-86 1780 (June 1961)

[9] Shelton, H, 'Experiments on atom and ion emission from porous tungsten," *ARS Progress in Astronautics and Rocketry Electric Propulsion Development,* edited by E Stuhlinger (Academic Press Inc, New York, 1963), Vol 9 pp 219–228

[10] Kuskevics G, "Criteria and a graphical method for optimization of cesium surface ionizer materials," AIAA J **1,** 1455–1458 (1963)

[11] Taylor, J B and Langmuir, I, 'The evaporation of atoms, ions and electrons from cesium films on tungsten," Phys. Rev **44,** 423–458 (1933)